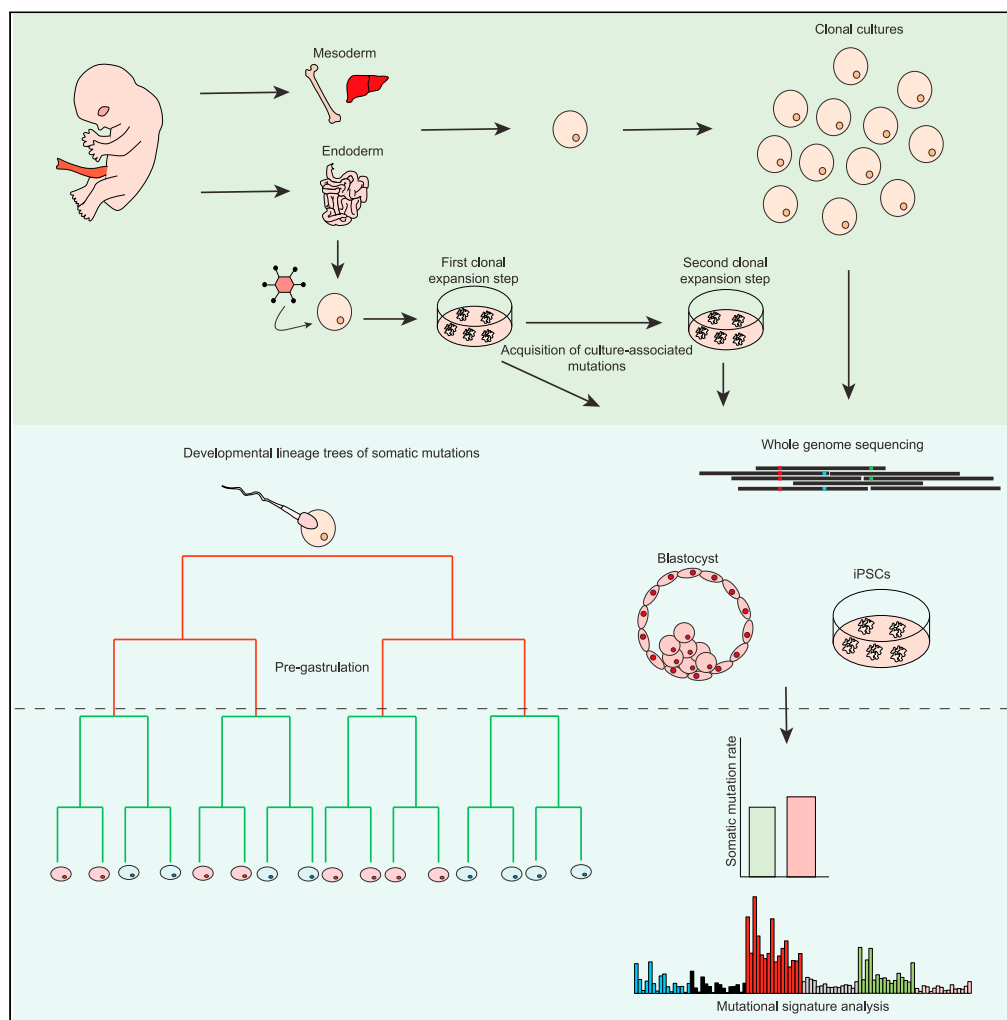# iScience

Article

Human induced pluripotent stem cells display a similar mutation burden as embryonic pluripotent cells *in vivo*

Karlijn A.L.
Hasaart, Freek
Manders, Joske
Ubels, ..., Ewart
Kuijk, Susana M.
Chuva de Sousa
Lopes, Ruben van
Boxtel

R.vanBoxtel@
prinsesmaximacentrum.nl

Highlights

Shared mutations in fetal cells allow pre-gastrulation mutation rate estimation

Human pluripotent cells have an *in vivo* mutation rate of 1.65 mutations per division

iPSCs generated from fetal cells show a similar mutation rate in hypoxic conditions

Similar mutational processes are active in iPSCs and pre-gastrulation embryonic cells

Article

Human induced pluripotent stem cells display a similar mutation burden as embryonic pluripotent cells *in vivo*

Karlijn A.L. Hasaart,[1,2] Freek Manders,[1,2] Joske Ubels,[1,2] Mark Verheul,[1,2] Markus J. van Roosmalen,[1,2] Niels M. Groenen,[1,2] Rurika Oka,[1,2] Ewart Kuijk,[2,3] Susana M. Chuva de Sousa Lopes,[4] and Ruben van Boxtel[1,2,5,*]

SUMMARY

Induced pluripotent stem cells (iPSCs) hold great promise for regenerative medicine, but genetic instability is a major concern. Embryonic pluripotent cells also accumulate mutations during early development, but how this relates to the mutation burden in iPSCs remains unknown. Here, we directly compared the mutation burden of cultured iPSCs with their isogenic embryonic cells during human embryogenesis. We generated developmental lineage trees of human fetuses by phylogenetic inference from somatic mutations in the genomes of multiple stem cells, which were derived from different germ layers. Using this approach, we characterized the mutations acquired pre-gastrulation and found a rate of 1.65 mutations per cell division. When cultured in hypoxic conditions, iPSCs generated from fetal stem cells of the assessed fetuses displayed a similar mutation rate and spectrum. Our results show that iPSCs maintain a genomic integrity during culture at a similar degree as their pluripotent counterparts do *in vivo*.

INTRODUCTION

Human pluripotent stem cells resemble the pluripotent epiblast of the early post-implantation embryo in the capacity to differentiate toward all three germ layers and any somatic cell type (Courtot et al., 2014; Lau et al., 2020; Yamanaka, 2020). Human pluripotent stem cell lines can be generated from the inner cell mass of blastocyst stage embryos or generated from more differentiated somatic cells using exogenous introduction of the four Yamanaka transcription factors (*POU5F1, SOX2, KLF4, MYC*) (Takahashi and Yamanaka, 2006).

In the last decades, induced pluripotent stem cells (iPSCs) have extensively been used for disease modeling and drug discovery (Rowe and Daley, 2019). Moreover, iPSCs are an attractive source for regenerative medicine, as they can be generated from the patient's own cell, and the first clinical trials for stem cell therapies have recently been launched (Yamanaka, 2020). However, previous research has shown that stem cells in culture, such as iPSCs, acquire mutations, which can cause genetic safety issues and has hampered the use of stem cell therapies in clinic (Kucab et al., 2019; Kuijk et al., 2020; Rouhani et al., 2016; Thompson et al., 2020). For example, *TP53* mutations, base substitutions, and duplications of chromosomes 1, 12, 17, and 20 are often identified in iPSCs (Kuijk et al., 2020; Laurent et al., 2011; Martins-Taylor et al., 2011; Merkle et al., 2017). These findings suggest that iPSCs in culture may suffer from enhanced genetic instability. However, stem cells also accumulate mutations during normal life (Blokzijl et al., 2016; Hasaart et al., 2020; Lee-Six et al., 2018; Mitchell et al., 2021; Moore et al., 2021; Osorio et al., 2018). To which extent the *in vitro* mutation accumulation in iPSCs varies from the natural genetic instability of pluripotent and totipotent embryonic cells *in vivo* remains unknown.

Here, we directly compared the *in vitro* mutation accumulation in iPSCs with the mutation burden of their isogenic embryonic cells during human embryogenesis. For this, we cataloged the somatic mutations acquired pre-gastrulation in four human fetuses using a phylogenetic approach and generated iPSCs of the same stem cells to determine culture-associated mutagenesis. We show that iPSCs, when cultured under hypoxic conditions to reduce culture-associated mutations (Kuijk et al., 2020; Li and Marbán, 2010), maintain a similar genetic integrity as their embryonic counterparts do *in vivo*.

[1]Princess Máxima Center for Pediatric Oncology, Heidelberglaan 25, 3584 CS Utrecht, the Netherlands

[2]Oncode Institute, Jaarbeursplein 6, 3521 AL Utrecht, the Netherlands

[3]Center for Molecular Medicine, University Medical Center Utrecht, Universiteitsweg 100, 3584 CG Utrecht, the Netherlands

[4]Department of Anatomy and Embryology, Leiden University Medical Center, 2333 ZC Leiden, the Netherlands

[5]Lead contact

*Correspondence:
R.vanBoxtel@
prinsesmaximacentrum.nl

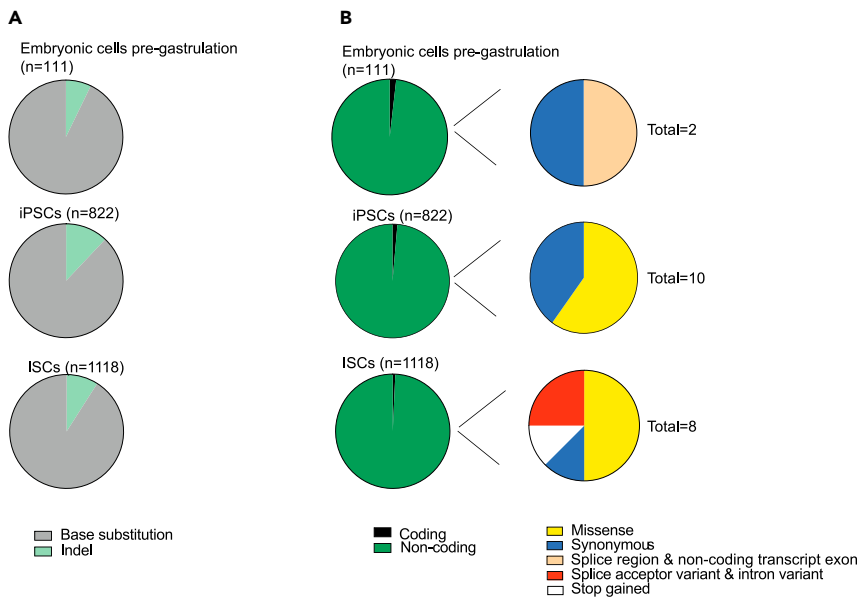https://doi.org/10.1016/j.isci.2022.103736

Figure 1. Identified mutations in embryonic cells pre-gastrulation and culture-associated mutations in iPSCs and fetal ISCs

(A) Pie charts representing the relative number of identified single base substitutions and indels.

(B) Pie charts representing the relative number of identified mutations affecting protein-coding regions of the genome (left) and relative number of protein-coding mutations causing missense, synonymous, stop gained, splice region and non-coding transcript exon, and splice acceptor and intron mutations (right) (Tables S1 and S2).

RESULTS

Mutation accumulation during early embryogenesis

Somatic mutations acquired by a cell are propagated to their future progeny. Therefore, mutations acquired during early embryogenesis will still be present in the genomes of adult cells, unless these are deleterious (Behjati et al., 2014; Ju et al., 2017; Lee-Six et al., 2018; Moore et al., 2021; Osorio et al., 2018). In addition, mutations shared by multiple cells derived from different germ layers of the same individual were acquired by an ancestral pluripotent or totipotent progenitor (Ju et al., 2017). We used this principle to determine the mutation rate pre-gastrulation during early human embryonic development. For this, we performed whole-genome sequencing (WGS) of multiple endoderm-derived intestinal stem cells (ISCs), mesoderm-derived hematopoietic stem and progenitor cells (HSPCs), and ectoderm/mesoderm-derived bulk skin of the same fetuses and constructed developmental lineage trees (Figure S1). To obtain sufficient DNA of a single cell for WGS, we clonally expanded the fetal stem cells *in vitro* (Hasaart et al., 2020). This approach allowed us to assess all mutations in the parental cell. We used DNA of bulk skin, of the same fetuses to control for germline mutations. Mutations that were acquired during the *in vitro* clonal expansion step could be excluded based on their low variant allele frequency (VAF) (Huber et al., 2019; Jager et al., 2017). Of note, we focused on mutations that were shared by multiple fetal cells of different germ layers and therefore accumulated *in vivo* in a shared ancestral cell, which was present during early embryogenesis pre-gastrulation.

In total, we sequenced 23 ISCs and 38 HSPCs of fetuses that were aborted because of the presence of a constitutive trisomy of chromosome 21 (T21; n = 2) or without medical indication (n = 2). Of note, the two latter fetuses were karyotypically normal (D21). In each fetus we identified 10–40 somatic mutations that were acquired before gastrulation (Figures 1A and 2A–2D). Of these, two mutations were located in protein coding sequences but were not identified as potential cancer driver mutations (Figure 1B and Table 1). Mutations that are acquired pre-gastrulation are present in the upper branches of a developmental lineage tree and can therefore be used to determine the early somatic mutation rate (Figures 2A–2D). Furthermore, mutations acquired during the same cell division will have a comparable VAF in bulk skin. In contrast, mutations acquired in subsequent cell divisions will have a lower VAF in bulk skin, assuming that no selection or genetic drift of embryonic clones took place (Ju et al., 2017). Some branch points are converted to polytomies, which suggests that during embryonic development, cell divisions have occurred without the
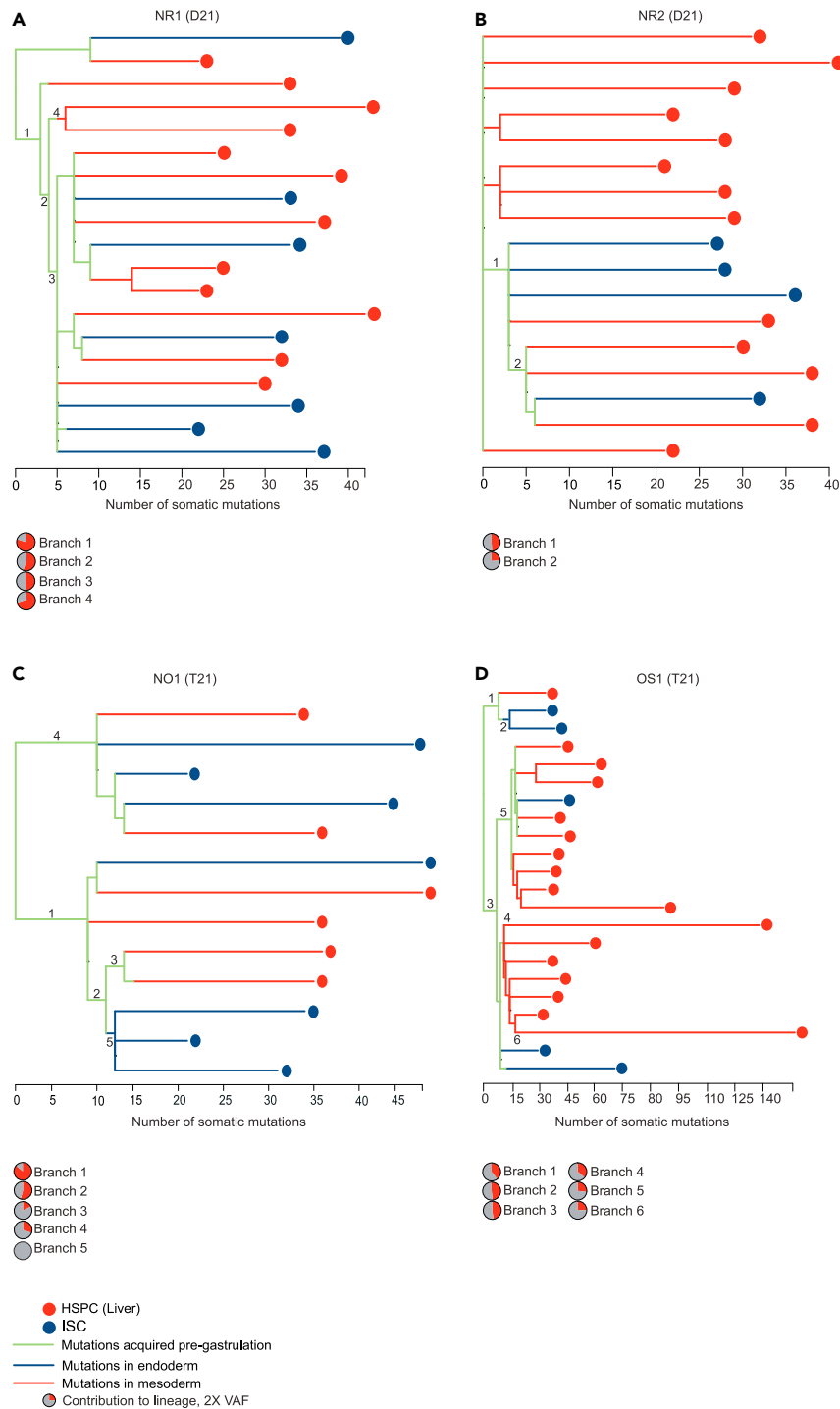
Figure 2. Developmental lineage trees of fetal stem cells derived from different germ layers

(A–D) Developmental lineage trees of four human fetuses (T21; n = 2, D21; n = 2) to show the clonal relationship of single intestinal stem cells (ISC) and single hematopoietic stem and progenitor cells (HSPC) (23 ISCs and 38 HSPCs). Each tip represents a single expanded cell. The green lines represent somatic mutations acquired pre-gastrulation, whereas blue lines represent somatic mutations present in the endoderm and red lines somatic mutations present in the mesoderm. Cell divisions in the branches indicated with a number are used to determine the somatic mutation rate pre-gastrulation. The pie charts represent the median contribution of the contributing mutations to bulk skin. Only the pie charts of the mutations acquired in cell divisions used to determine the somatic mutation rate pre-gastrulation are shown. The red parts indicate the contribution of the mutations to bulk skin (Figures S2B–S2E).

Table 1. Mutations located in protein coding regions in embryonic cells pre-gastrulation, iPSCs, and fetal ISCs in culture

Variant	Position	Gene	Predicted effect	Mutation type	Cell type	Fetus
G>C	1:203800025	ZBED6	Moderate	Missense	iPSC	NR2 (D21)
G>A	1:203800166	ZBED6	Moderate	Missense	iPSC	NR2 (D21)
G>A	1:203800309	ZBED6	Low	Synonymous	iPSC	NR2 (D21)
G>A	3:132475016	DNAJC13	Moderate	Missense	iPSC	NR2 (D21)
G>A	1:53277029	LRP8	Low	Synonymous	iPSC	NR2 (D21)
G>A	2:109501510	SH3RF3	Moderate	Missense	iPSC	NR2 (D21)
G>A	19:15110164	SYDE1	Low	Synonymous	iPSC	OS1 (T21)
G>A	1:16992069	ATP13A2	Moderate	Missense	iPSC	OS1 (T21)
G>A	12:49049850	KMTD2	Low	Synonymous	iPSC	OS1 (T21)
G>A	8:127740738	MYC	Moderate	Missense	iPSC	NR1 (D21)
C>T	13:85794862	SLITRK6	Low	Synonymous	Pre-gastrulation	NR1 (D21)
C>T	3:126072855	KLF15	Low	Splice region & non-coding transcript exon	Pre-gastrulation	NR1 (D21)
T>C	20:45222766	SMEG2	Low	Synonymous	ISC	NR2 (D21)
A>T	20:45222776	SMEG2	Moderate	Missense	ISC	NR2 (D21)
G>A	5:168666663	SLIT3	High	Stop gained	ISC	NR2 (D21)
C>T	X:37572088	LANCL3	Moderate	Missense	ISC	NR2 (D21)
G>A	16:2530837	CEMP1	Low	Synonymous	ISC	OS1 (T21)
C>T	2:179945716	CWC22	High	Splice acceptor & intron	ISC	OS1 (T21)
G>A	2:179945716	PER3	Moderate	Missense	ISC	NR1 (D21)
T>G	8:68060689	PREX2	Moderate	Missense	ISC	NR1 (D21)

The table shows all mutations located in protein coding regions and the estimated effect based on snpEff. The mutations in *MYC* and *PREX2* are considered as potential cancer driver mutations because these were annotated with a moderate effect and were present in the cancer gene census.

acquisition of any somatic mutation (Figures 2A–2D). Importantly, mutations that were acquired in lineages, which were lost during development, cannot be annotated. We used the mutations in the different branches of the constructed phylogenies to determine the pre-gastrulation somatic mutation rate during human embryogenesis (see STAR Methods). In total, we could use 17 independent cell divisions, which all took place before gastrulation to estimate the somatic mutation rate pre-gastrulation (see STAR Methods). Of note, more cell divisions took place before gastrulation; however, not all can be used for the estimation (see STAR Methods). To determine the pre-gastrulation somatic mutation rate as accurate as possible, we only included cell divisions in which the VAF of the mutations in the daughter cells was equal to the VAF of the mutations in the mother cell. We estimated a pre-gastrulation somatic mutation rate of 1.65 ± 0.93 (SD) mutations per cell division (Figure 3A). This mutation rate is in line with previous studies, in which the early embryonic mutation rate was determined by sequencing of clonal expansions of adult individuals (Coorens et al., 2021; Lee-Six et al., 2018; Park et al., 2021). Previously, we have shown an increased somatic mutation load in multipotent stem and progenitor cells in T21 fetuses (Hasaart et al., 2020). However, the mutation rate pre-gastrulation is similar between T21 and karyotypically normal human fetuses (Figure S2A). To validate our finding, we estimated the somatic mutation rate using a complementary approach. We performed deep targeted sequencing for the mutations, which we identified in the fetal clones, on bulk tissues derived from different germ layers of the assessed fetuses (Figure S1). We examined endoderm-derived early passage (P0) bulk intestinal organoid cultures, ectoderm/mesoderm-derived bulk skin of all four fetuses, and mesoderm-derived spleen of one T21 fetus (Figures S2B–S2E). Using this approach, we found a similar somatic mutation rate pre-gastrulation (Figure S2F).

Mutation accumulation in iPSCs

We used the ISC cultures of the fetuses, which we analyzed by WGS, to generate isogenic iPSC lines (Figure S1). Using RNA sequencing analysis, we demonstrated that the iPSC lines show a different transcriptional profile compared to tp the ISC cultures. Moreover, we confirmed a similar expression profile of the
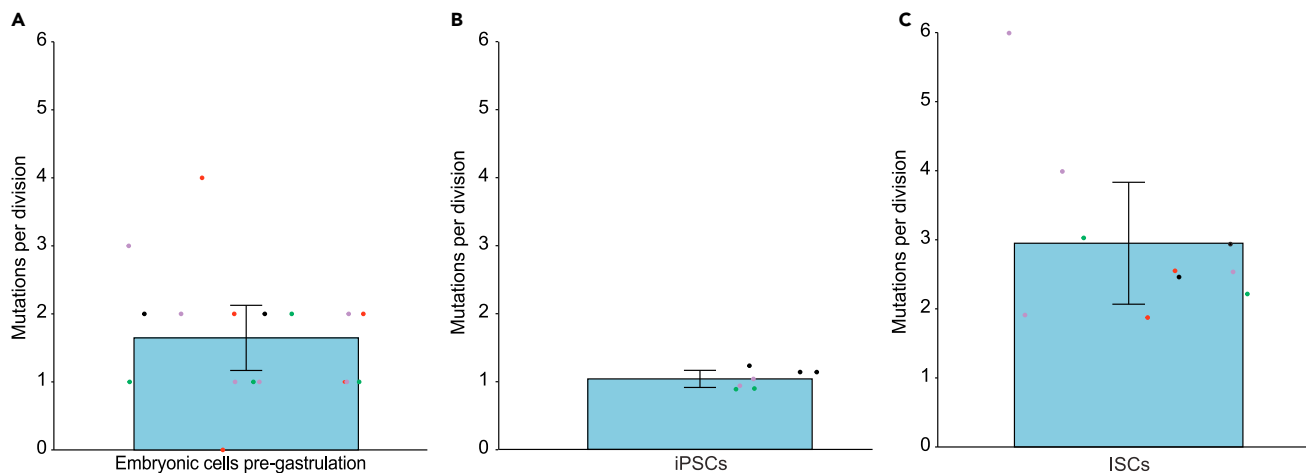
Figure 3. The somatic mutation rate of embryonic cells pre-gastrulation, iPSCs, and fetal ISCs in culture

(A) The somatic mutation rate (mutations/cell division) pre-gastrulation. Mean 1.65 ± 0.93 SD. Colored dots indicate a cell division pre-gastrulation occurred in one of the four fetuses (T21; n = 2, D21; n = 2) (Figures S2A and S2F).

(B) The somatic mutation rate (mutations/cell division) of clonal iPSC lines during hypoxic cell culture. Mean 1.03 ± 0.14 SD. Colored dots indicate the seven clonal iPSC cell lines derived from the fetal ISCs of the fetuses (T21; n = 1, D21; n = 2). The mutation rate of embryonic cells pre-gastrulation and iPSCs did not differ significantly (Wilcoxon rank-sum test p = 0.12) (Figures S3, S4, and S5A).

(C) The somatic mutation rate (mutations/cell division) of clonal fetal ISCs, used to generate iPSCs, during normoxic cell culture. Mean 2.95 ± 1.23 SD. Colored dots indicate the 10 clonal fetal ISCs derived from the 4 fetuses (T21; n = 2, D21; n = 2). The culture-associated mutation rate of iPSCs and fetal ISCs is significantly different (Wilcoxon rank-sum test p = 0.0001) (Figure S5B). All data are represented as mean and 95% confidence interval.

generated iPSCs and human embryonic stem cells (hESCs), suggesting that the reprogramming was successful (Figure S3) (Kuijk et al., 2020). We generated clonal iPSC cultures (see STAR Methods), which were analyzed by WGS to catalog the mutations present in the parental cell. These clonal iPSC lines were kept in culture for approximately 3 months to allow somatic mutations to accumulate. Cells were cultured under hypoxic conditions (3% O_2), and all procedures, such as medium preparation, medium change, and passaging, were performed under hypoxic conditions to reduce the acquisition of mutations in culture (Kuijk et al., 2020; Li and Marbán, 2010; Thompson et al., 2020). Subsequently, a second clonal expansion step was performed to generate sub-clonal iPSC lines, which were also subjected to WGS analysis. By subtracting the somatic mutations present in the parental clone from those observed in the matching sub-clone, we were able to accurately assess the mutation burden associated with *in vitro* expansion of iPSCs (Jager et al., 2017). We subjected seven clone-subclone pairs to WGS analysis, which were derived from one of the T21 and the two D21 fetuses. In these clonal iPSC cell lines, we identified 723 culture-associated base substitutions and 99 culture-associated insertions-deletions (indels) (Figure 1A). In one of the clonal iPSC lines, which was derived from a D21 fetus, a part of chromosome 18 was deleted (Figure S4A). This deletion was sub-clonally present in the culture and was absent in the sub-clone. Besides that, we did not observe any karyotype abnormalities in the other iPSC lines (Figure S4A). Of all mutations that accumulated between the two subsequent clonal expansion steps, 10 mutations were located in protein-coding sequences (Figure 1B and Table 1). Of these, one was considered as a potential cancer driver gene and was located in the oncogene *MYC*. This mutation was found in the matching sub-clone, which was derived from the clonal iPSC culture with a partial deletion of chromosome 18.

To accurately estimate the culture-associated mutation rate, we determined the cell cycle length of the iPSCs by pulse chase of 5-ethynyl-2'-deoxyuridine (EdU) followed by measuring co-staining with DAPI and the mitosis marker phosphorylated histone 3 (pH3) (see STAR Methods). Using this approach, we found that iPSCs divide every 18 hours (Figure S4B), indicating that iPSCs acquire 1.03 ± 0.14 (SD) mutations per cell division under reduced oxygen conditions (Figures 3B and S5A). The observed cell division time is in line with a previous study, where the cell cycle length of iPSCs under normoxic culture conditions was determined to be 16–18 hours (Ghule et al., 2011). This finding suggests that the hypoxic culture conditions we applied had no effect on the cell division time.

To compare the culture-associated mutation rate of iPSCs with the culture-associated mutation rate of their source cells, we performed sequential single cell expansion steps of the ISC clones (Figure S1). For this, we used the clonal ISCs of the same fetuses to determine the culture-associated mutation rate under normoxic culture conditions. Before the generation of sub-clonal fetal ISC lines, clonal ISC cultures were kept in culture for approximately 1.5 months in order to accumulate sufficient culture-associated mutations to accurately determine an *in vitro* mutation burden. The sub-clonal fetal ISC lines were subjected to WGS and a similar filtering method was applied as described above. In total, we subjected 10 sub-clones to WGS derived from 8 clonal ISCs of 2 D21 fetuses and 2 T21 fetuses. We identified 1,017 culture-associated base substitutions and 101 cultured-associated indels (Figure 1A). Of all culture-associated mutations, eight mutations were located in protein-coding sequences (Figure 1B and Table 1). One mutation was located in the oncogene *PREX2* and therefore might represent a potential cancer driver mutation. The cell division length of ISCs in culture has been previously determined to be 26 hours, indicating that fetal ISCs acquire 2.95 ± 1.23 (SD) mutations per cell division under normoxic culture conditions (Drost et al., 2017) (Figures 3C and S5B).

Overall, we conclude that cultured iPSCs display a similar mutation rate *in vitro* as their pluripotent and totipotent cells do *in vivo* (Wilcoxon rank-sum test p = 0.12), suggesting that the culture system has no or only limited additive mutagenic effects. Moreover, iPSCs derived from fetal ISCs display a lower mutation rate in culture compared with the culture-associated mutation rate of their fetal source cells (Wilcoxon rank-sum test p = 0.0001).

Active mutational processes

Although the mutation rate in cultured iPSCs was similar to the mutation rate pre-gastrulation, the mutation spectra were slightly different (Figures 4A, 4B, and S6A), suggesting that that there is a difference in mutational processes acting on these cells. To obtain more insight in the mutational processes causing these mutations, we performed mutational signature analysis (see STAR Methods). The predominant mutational signature in both cultured iPSCs and embryonic cells *in vivo* was COSMIC signature SBS5 (Figures 4C, 4D, S6B, and S6C). More than 60% of the observed mutations in embryonic cells pre-gastrulation and more than 80% of culture-associated mutations in iPSCs could be attributed to this signature (Figures 4C, 4D, S6B, and S6C). The remainder of the mutations in both cell types could be attributed to COSMIC signature SBS1 (Figures 4C, 4D, S6B, and S6C). This signature is caused by the spontaneous deamination of methylated cytosines and may represent a mutational clock in terms of cell division or time (Alexandrov et al., 2015; Blokzijl et al., 2016; Koh et al., 2021). Embryonic cells pre-gastrulation show more activity of the mutational process underlying this mutational signature, which is line with the observed increased proportion of C>T changes at CpG (Figure 4A). During embryonic development cells display high levels of proliferation to give rise to cells of all germ layers in a short time, which may explain the increased contribution of SBS1. In conclusion, these findings indicate that the main mutational processes in cultured iPSCs and embryonic cells pre-gastrulation are similar, which support our initial observation that the mutation burden in hypoxic-cultured iPSCs and totipotent and pluripotent cells *in vivo* is highly similar. However, the contribution of SBS1 and SBS5 to the mutation spectra of embryonic cells pre-gastrulation and iPSCs is slightly different.

DISCUSSION

Previous studies have shown that both multipotent stem cells and iPSCs acquire mutations during culture, which may compromise the clinical use of these cells (Kuijk et al., 2020; Laurent et al., 2011; Martins-Taylor et al., 2011; Merkle et al., 2017). Indeed, it has been demonstrated that multipotent adult stem cells can have an increased mutation rate *in vitro* as compared with their *in vivo* counterpart (Kuijk et al., 2020). For example, adult ISCs *in vitro* have a nearly 40-fold increased mutation rate as compared to the mutation rate *in vivo*. In contrast, our study demonstrates that iPSCs, when cultured under hypoxic conditions, display a similar mutation burden as their *in vivo* totipotent and pluripotent counterparts. In addition, the culture-associated mutation rate of iPSCs is lower compared to the culture-associated mutation rate of their fetal source cells. These results indicate that iPSCs maintain their natural genomic stability during hypoxic cell culture. The observed culture-associated mutation rate of iPSCs cultured in hypoxic conditions are in line with two other studies measuring the mutation rate of iPSCs and hESC during hypoxic cell culture (Kuijk et al., 2020; Thompson et al., 2020). These and our results demonstrate that hypoxic cell culture reduces the number of culture-associated mutations (Kuijk et al., 2020; Rouhani et al., 2016; Thompson et al., 2020). The levels of oxygen have also been reported to reduce the methylation status of hESC, decrease spontaneous differentiation, and promote the differentiation capacity toward other cell types
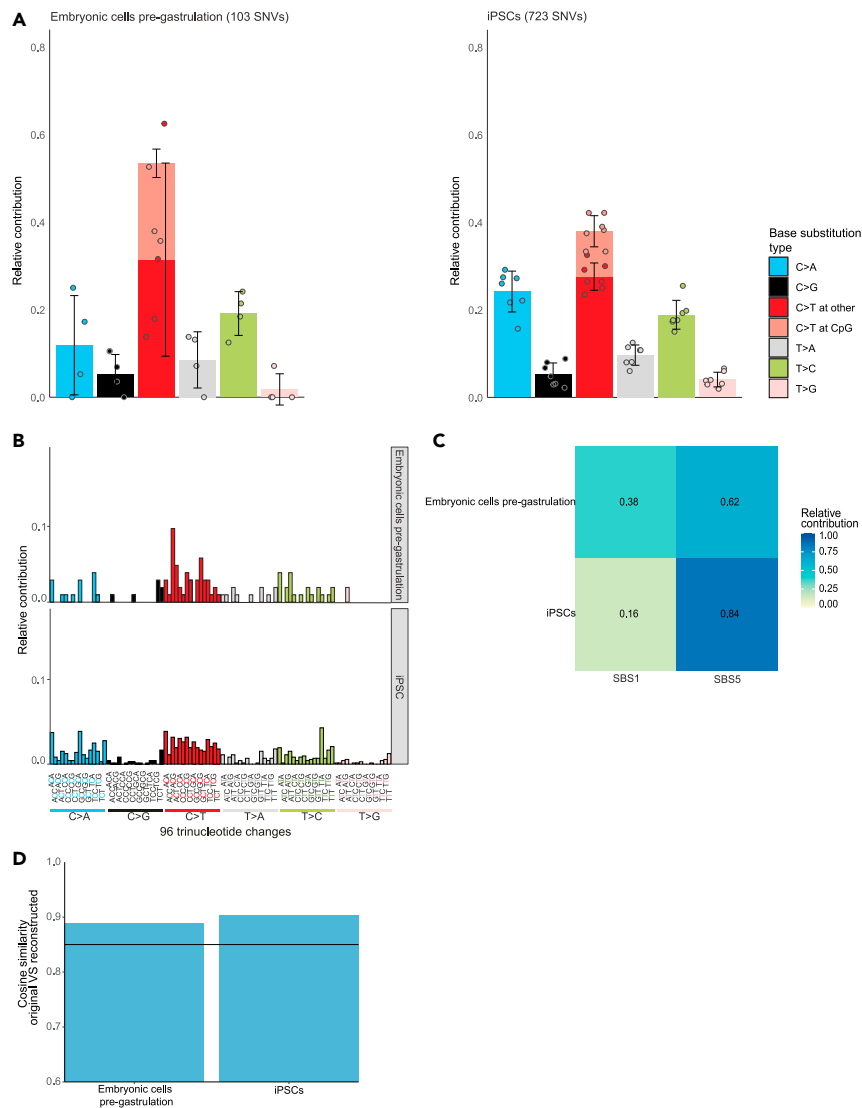
Figure 4. Active mutational processes

(A) Relative contribution of the indicated base substitutions to the mutational spectra of embryonic cells pre-gastrulation. Dots represent the four fetuses (T21; n = 2, D21; n = 2, 23 ISCs and 38 HSPCs) (left) Relative contribution of the indicated base substitutions to the mutational spectra of iPSCs. Dots represent the seven iPSC clones derived from the fetal ISCs of three fetuses (T21; n = 1, D21; n = 2) (right). Data are represented as mean ± SD. The mutational spectra differ significantly (chi-squared test p = 0.017).

(B) The 96-trinucleotide profiles of embryonic cells pre-gastrulation and iPSCs. Cosine similarity between the two profiles is 0.74.

(C) The relative contribution of each mutational signature to the spectra of base substitutions.

(D) The cosine similarity between the mutational spectra and the mean reconstructed profiles (Figure S6).

(Ezashi et al., 2005; Fynes et al., 2014; Thompson et al., 2020). Together, this suggests that hypoxic cell culture is beneficial for the genomic integrity of pluripotent cells. Of note, we show that karyotypically abnormal (T21) iPSCs remain stable during culture, whereas their parental fetal ISCs are less stable *in vivo* compared with karyotypically normal ISCs (Hasaart et al., 2020). This finding implies that iPSCs generated from a disease model remain stable during culture as well. Of note, the reprogramming process of somatic cells toward pluripotency is a stressful process and a G1/S cell cycle checkpoint deficiency during the initial phases of reprogramming causes an increase in base substitutions during this limited time frame (Araki et al., 2020; Bhutani et al., 2016; Kida et al., 2015; Sugiura et al., 2014). Therefore, the initial phase of

iPSC differentiation toward other lineages might also result in an increased mutational burden during a limited time frame.

Oncogenic mutations, such as *TP53*, occur once in every $\sim 2.0 \times 10^9$ cultured iPSCs according to previous research (Kuijk et al., 2020; Merkle et al., 2017). Indeed, we observed a mutation in oncogene *MYC* and a subclonal deletion of a part of chromosome 18 in the matching clonal iPSC cell line. Nevertheless, during fetal development and even during early embryogenesis, cells can also acquire oncogenic mutations (Custers et al., 2021; Greaves, 2018; Williams et al., 2020). For example, sacrococcygeal teratomas, the most common tumor type in newborns, arise from germ cells and can recapitulate cells of all three germ layers (Manes, 1976; Moore et al., 2003). Germ cells arise around the time of gastrulation and are induced from the epiblast, suggesting that the cell of origin of these tumors arose at the time of pluripotency (Nicholls et al., 2019). This suggests that the acquisition of oncogenic mutations in pluripotent cells *in vivo* and *in vitro* can be a "natural" event.

Overall, we conclude that cultured iPSCs maintain a genomic integrity during hypoxic cell culture at a similar degree as embryonic cells pre-gastrulation *in vivo*. Therefore, iPSCs may safely be used for regenerative medicine in terms of genome stability. We emphasize to culture iPSCs under hypoxic culture conditions to reduce the number of culture-associated mutations. However, since it is still possible for a cancer driver mutation to occur, we recommend that parental somatic cells and cultured iPSCs are screened for oncogenic mutations before they are used for stem cell therapies in patients.

Limitations of the study

In this study, we estimated the somatic mutation rate pre-gastrulation of four human fetuses using a phylogenetic inference approach. Some branch points are converted to polytomies, suggesting that cell divisions have occurred without the acquisition of any somatic mutation. Importantly, mutations that were acquired in lineages, which were lost during development, cannot be annotated. To estimate the somatic mutation rate pre-gastrulation as accurately as possible, we only included cell divisions in which the VAF of the mutations in the daughter cells was equal to the VAF of the mutations in the mother cell. However, we stress that the obtained somatic mutation rate pre-gastrulation is an estimation. In addition, the iPSCs in this study are cultured under hypoxic culture conditions, because previous studies have shown that this reduces the number of culture-associated mutations. Nevertheless, the vast majority of laboratories and cell therapy companies make use of normoxic culture conditions. Therefore, the results obtained in this study might not be applicable to iPSCs cultured in normoxic culture conditions.

STAR★METHODS

Detailed methods are provided in the online version of this paper and include the following:

- KEY RESOURCES TABLE
- RESOURCE AVAILABILITY
  - Lead contact
  - Materials availability
  - Data and code availability
- EXPERIMENTAL MODEL AND SUBJECT DETAILS
- METHOD DETAILS
  - Isolation and clonal cultures of HSPCs
  - Intestinal organoid cultures
  - iPSC culture
  - Cell cycle length of iPSCs
  - RNA sequencing
  - Genomic DNA isolation
  - Whole genome sequencing and read alignment
  - Somatic mutation calling and filtering
  - Targeted deep re-sequencing
  - Construction of developmental lineage tree
  - Mutation rate during early embryogenesis
  - Mutation rate of iPSCs and ISCs
  - Mutational profiles and signature analyses
- QUANTIFICATION AND STATISTICAL ANALYSIS

SUPPLEMENTAL INFORMATION

Supplemental information can be found online at https://doi.org/10.1016/j.isci.2022.103736.

AUTHOR CONTRIBUTIONS

K.A.L.H. performed sample preparation, FACS, RNA isolation, and ISC and HSPC cultures. K.A.L.H. and M.V. performed iPSC culture and DNA isolations. K.A.L.H. and N.M.G. performed EdU-PH3 stainings. M.V. performed library preparation and capture for targeted deep sequencing. E.K. generated iPSC cultures. K.A.L.H., F.M., J.U., M.J.v.R, and R.O. performed bioinformatic analyses. S.M.C.d.S.L collected fetal material. K.A.L.H. and R.B. wrote the manuscript. R.B. designed and supervised the study. All authors reviewed the manuscript.

DECLARATION OF INTERESTS

The authors declare no competing interests.

REFERENCES

Alexandrov, L.B., Jones, P.H., Wedge, D.C., Sale, J.E., Campbell, P.J., Nik-Zainal, S., and Stratton, M.R. (2015). Clock-like mutational processes in human somatic cells. Nat. Genet. *47*, 1402–1407.

Alexandrov, L.B., Kim, J., Haradhvala, N.J., Huang, M.N., Ng, A.W.T., Wu, Y., Boot, A., Covington, K.R., Gordenin, D.A., Bergstrom, E.N., et al. (2020). The repertoire of mutational signatures in human cancer. Nature *578*, 94–101.

Araki, R., Hoki, Y., Suga, T., Obara, C., Sunayama, M., Imadome, K., Fujita, M., Kamimura, S., Nakamura, M., Wakayama, S., et al. (2020). Genetic aberrations in iPSCs are introduced by a transient G1/S cell cycle checkpoint deficiency. Nat. Commun. *11*, 197.

Behjati, S., Huch, M., van Boxtel, R., Karthaus, W., Wedge, D.C., Tamuri, A.U., Martincorena, I., Petljak, M., Alexandrov, L.B., Gundem, G., et al. (2014). Genome sequencing of normal cells reveals developmental lineages and mutational processes. Nature *513*, 422–425.

Benjamini, Y., and Hochberg, Y. (1995). Controlling the false discovery rate: a practical and powerful approach to multiple testing. J. R. Stat. Soc. Series B Methodol. *57*, 289–300.

Bhutani, K., Nazor, K.L., Williams, R., Tran, H., Dai, H., Džakula, Ž., Cho, E.H., Pang, A.W.C., Rao, M., Cao, H., et al. (2016). Whole-genome mutational burden analysis of three pluripotency induction methods. Nat. Commun. *7*, 1–8.

Blokzijl, F., de Ligt, J., Jager, M., Sasselli, V., Roerink, S., Sasaki, N., Huch, M., Boymans, S., Kuijk, E., Prins, P., et al. (2016). Tissue-specific mutation accumulation in human adult stem cells during life. Nature *538*, 260–264.

Blokzijl, F., Janssen, R., van Boxtel, R., and Cuppen, E. (2018). MutationalPatterns: comprehensive genome-wide analysis of mutational processes. Genome Med. *10*, 33.

Boeva, V., Popova, T., Bleakley, K., Chiche, P., Cappo, J., Schleiermacher, G., Janoueix-Lerosey, I., Delattre, O., and Barillot, E. (2012). Control-FREEC: a tool for assessing copy number and allelic content using next-generation sequencing data. Bioinformatics *28*, 423.

Cingolani, P., Platts, A., Wang, L.L., Coon, M., Nguyen, T., Wang, L., Land, S.J., Lu, X., and Ruden, D.M. (2012). A program for annotating and predicting the effects of single nucleotide polymorphisms, SnpEff: SNPs in the genome of Drosophila melanogaster strain w1118; iso-2; iso-3. Fly *6*, 80–92.

Coorens, T.H.H., Moore, L., Robinson, P.S., Sanghvi, R., Christopher, J., Hewinson, J., Przybilla, M.J., Lawson, A.R.J., Spencer Chapman, M., Cagan, A., et al. (2021). Extensive phylogenies of human development inferred from somatic mutations. Nature *597*, 387–392.

Courtot, A.M., Magniez, A., Oudrhiri, N., Féraud, O., Bacci, J., Gobbo, E., Proust, S., Turhan, A.G., and Bennaceur-Griscelli, A. (2014). Morphological analysis of human induced pluripotent stem cells during induced differentiation and reverse programming. Biores. Open Access *3*, 206–216.

Custers, L., Khabirova, E., Coorens, T.H.H., Oliver, T.R.W., Calandrini, C., Young, M.D., Vieira Braga, F.A., Ellis, P., Mamanova, L., Segers, H., et al. (2021). Somatic mutations and single-cell transcriptomes reveal the root of malignant rhabdoid tumours. Nat. Commun. *12*, 1407.

DePristo, M.A., Banks, E., Poplin, R., Garimella, K.V., Maguire, J.R., Hartl, C., Philippakis, A.A., del Angel, G., Rivas, M.A., Hanna, M., et al. (2011). A framework for variation discovery and genotyping using next-generation DNA sequencing data. Nat. Genet. *43*, 491–498.

Drost, J., Van Boxtel, R., Blokzijl, F., Mizutani, T., Sasaki, N., Sasselli, V., de Ligt, J., Behjati, S., Grolleman, J.E., van Wezel, T., et al. (2017). Use of CRISPR-modified human stem cell organoids to study the origin of mutational signatures in cancer. Science *358*, 234–238.

Ewels, P., Mans, M., Lundin, S., and Kaller, M. (2016). MultiQC: summarize analysis results for multiple tools and samples in a single report. Bioinformatics *32*, 3047–3048.

Ezashi, T., Das, P., and Roberts, R.M. (2005). Low O2 tensions and the prevention of differentiation of hES cells. Proc. Natl. Acad. Sci. U S A *102*, 4783–4788.

Fynes, K., Tostoes, R., Ruban, L., Weil, B., Mason, C., and Veraitch, F.S. (2014). The differential effects of 2% oxygen preconditioning on the subsequent differentiation of mouse and human

pluripotent stem cells. Stem Cells Dev. 23, 1910–1922.

Gerstung, M., Papaemmanuil, E., and Campbell, P.J. (2014). Subclonal variant calling with multiple samples and prior knowledge. Bioinformatics 30, 1198.

Ghule, P.N., Medina, R., Lengner, C.J., Mandeville, M., Qiao, M., Dominski, Z., Lian, J.B., Stein, J.L., van Wijnen, A.J., and Stein, G.S. (2011). Reprogramming the pluripotent cell cycle: restoration of an abbreviated G1 phase in human induced pluripotent stem (iPS) cells. J. Cell Physiol. 226, 1149–1156.

Greaves, M. (2018). A causal mechanism for childhood acute lymphoblastic leukaemia. Nat. Rev. Cancer 18, 471–484.

Hasaart, K.A.L., Manders, F., van der Hoorn, M.L., Verheul, M., Poplonski, T., Kuijk, E., de Sousa Lopes, S.M.C., and van Boxtel, R. (2020). Mutation accumulation and developmental lineages in normal and down syndrome human fetal haematopoiesis. Sci. Rep. 10, 12991.

Huber, A.R., Manders, F., Oka, R., and van Boxtel, R. (2019). Characterizing mutational load and clonal composition of human blood. J. Vis. Exp. https://doi.org/10.3791/59846.

Jager, M., Blokzijl, F., Sasselli, V., Boymans, S., Janssen, R., Besselink, N., Clevers, H., van Boxtel, R., and Cuppen, E. (2017). Measuring mutation accumulation in single human adult stem cells by whole-genome sequencing of organoid cultures. Nat. Protoc. 13, 59–78.

Ju, Y.S., Martincorena, I., Gerstung, M., Petljak, M., Alexandrov, L.B., Rahbari, R., Wedge, D.C., Davies, H.R., Ramakrishna, M., Fullam, A., et al. (2017). Somatic mutations reveal asymmetric cellular dynamics in the early human embryo. Nature 543, 714–718.

Kida, Y.S., Kawamura, T., Downes, M., Evans Correspondence, R.M., Article, S., Wei, Z., Sogo, T., Jacinto, S., Shigeno, A., Kushige, H., et al. (2015). ERRs mediate a metabolic switch required for somatic cell reprogramming to pluripotency cell stem cell ERRs mediate a metabolic switch required for somatic cell reprogramming to pluripotency. Cell Stem Cell 16, 547–555.

Koh, G., Degasperi, A., Zou, X., Momen, S., and Nik-Zainal, S. (2021). Mutational signatures: emerging concepts, caveats and clinical applications. Nat. Rev. Cancer 21, 1–19.

Kucab, J.E., Zou, X., Morganella, S., Joel, M., Nanda, A.S., Nagy, E., Gomez, C., Degasperi, A., Harris, R., Jackson, S.P., et al. (2019). A compendium of mutational signatures of environmental agents. Cell 177, 821–836.e16.

Kuijk, E., Jager, M., van der Roest, B., Locati, M.D., van Hoeck, A., Korzelius, J., Janssen, R., Besselink, N., Boymans, S., van Boxtel, R., et al. (2020). The mutational impact of culturing human pluripotent and adult stem cells. Nat. Commun. 11, 1–12.

Lau, K.X., Mason, E.A., Kie, J., de Souza, D.P., Kloehn, J., Tull, D., McConville, M.J., Keniry, A., Beck, T., Blewitt, M.E., et al. (2020). Unique properties of a subset of human pluripotent stem cells with high capacity for self-renewal. Nat. Commun. 11, 1–18.

Laurent, L.C., Ulitsky, I., Slavin, I., Tran, H., Schork, A., Morey, R., Lynch, C., Harness, J.v., Lee, S., Barrero, M.J., et al. (2011). Dynamic changes in the copy number of pluripotency and cell proliferation genes in human ESCs and iPSCs during reprogramming and time in culture. Cell Stem Cell 8, 106–118.

Lee-Six, H., Øbro, N.F., Shepherd, M.S., Grossmann, S., Dawson, K., Belmonte, M., Osborne, R.J., Huntly, B.J.P., Martincorena, I., Anderson, E., et al. (2018). Population dynamics of normal human blood inferred from somatic mutations. Nature 561, 473–478.

Li, H., and Durbin, R. (2010). Fast and accurate long-read alignment with Burrows–Wheeler transform. Bioinformatics 26, 589–595.

Li, T.S., and Marbán, E. (2010). Physiological levels of reactive oxygen species are required to maintain genomic stability in stem cells. Stem Cells 28, 1178–1185.

Li, H., Handsaker, B., Wysoker, A., Fennell, T., Ruan, J., Homer, N., Marth, G., Abecasis, G., and Durbin, R.; 1000 Genome Project Data Processing Subgroup (2009). The sequence alignment/map format and SAMtools. Bioinformatics 25, 2078–2079.

Love, M.I., Huber, W., and Anders, S. (2014). Moderated estimation of fold change and dispersion for RNA-seq data with DESeq2. Genome Biol. 15, 1–21.

Lüdecke, D. (2018). Ggeffects: tidy data frames of marginal effects from regression models. J. Open Source Softw. 3, 772.

Manes, C. (1976). Summation: model systems for the study of oncodevelopmental gene expression—murine teratocarcinoma. Cancer Res. 36, 4238.

Martins-Taylor, K., Nisler, B.S., Taapken, S.M., Compton, T., Crandall, L., Montgomery, K.D., Lalande, M., and Xu, R.H. (2011). Recurrent copy number variations in human induced pluripotent stem cells. Nat. Biotechnol. 29, 488–491.

Merkle, F.T., Ghosh, S., Kamitaki, N., Mitchell, J., Avior, Y., Mello, C., Kashin, S., Mekhoubad, S., Ilic, D., Charlton, M., et al. (2017). Human pluripotent stem cells recurrently acquire and expand dominant negative P53 mutations. Nature 545, 229–233.

Mitchell, E., Chapman, M.S., Williams, N., Dawson, K., Mende, N., Calderbank, E.F., Jung, H., Mitchell, T., Coorens, T., Spencer, D., et al. (2021). Clonal dynamics of haematopoiesis across the human lifespan. bioRxiv, 2021.08.16.456475.

Moore, L., Cagan, A., Coorens, T.H.H., Neville, M.D.C., Sanghvi, R., Sanders, M.A., Oliver, T.R.W., Leongamornlert, D., Ellis, P., Noorani, A., et al. (2021). The mutational landscape of human somatic and germline cells. Nature 597, 381–386.

Moore, S.W., Satgé, D., Sasco, A.J., Zimmermann, A., and Plaschkes, J. (2003). The epidemiology of neonatal tumours. Pediatr. Surg. Int. 19, 509–519.

Nicholls, P.K., Schorle, H., Naqvi, S., Hu, Y.C., Fan, Y., Carmell, M.A., Dobrinski, I., Watson, A.L.,

Carlson, D.F., Fahrenkrug, S.C., et al. (2019). Mammalian germ cells are determined after PGC colonization of the nascent gonad. Proc. Natl. Acad. Sci. U S A 116, 25677–25687.

Nik-Zainal, S., Van Loo, P., Wedge, D.C., Alexandrov, L.B., Greenman, C.D., Lau, K.W., Raine, K., Jones, D., Marshall, J., Ramakrishna, M., et al. (2012). The life history of 21 breast cancers. Cell 149, 994–1007.

Osorio, F.G., Rosendahl Huber, A., Oka, R., Verheul, M., Patel, S.H., Hasaart, K., de la Fonteijne, L., Varela, I., Camargo, F.D., and van Boxtel, R. (2018). Somatic mutations reveal lineage relationships and age-related mutagenesis in human hematopoiesis. Cell Rep. 25, 2308–2316.e4.

Paradis, E., Claude, J., and Strimmer, K. (2004). APE: Analyses of Phylogenetics and Evolution in R language. Bioinformatics 20, 289–290.

Park, S., Mali, N.M., Kim, R., Choi, J.-W., Lee, J., Lim, J., Park, J.M., Park, J.W., Kim, D., Kim, T., et al. (2021). Clonal dynamics in early human embryogenesis inferred from somatic mutation. Nature 597, 393–397.

Rouhani, F.J., Nik-Zainal, S., Wuster, A., Li, Y., Conte, N., Koike-Yusa, H., Kumasaka, N., Vallier, L., Yusa, K., and Bradley, A. (2016). Mutational history of a human cell lineage from somatic to induced pluripotent stem cells. PLoS Genet. 12, e1005932.

Rowe, R.G., and Daley, G.Q. (2019). Induced pluripotent stem cells in disease modelling and drug discovery. Nat. Rev. Genet. 20, 377–388.

Smigielski, E.M., Sirotkin, K., Ward, M., and Sherry, S.T. (2000). dbSNP: a database of single nucleotide polymorphisms. Nucleic Acids Res. 28, 352.

Sondka, Z., Bamford, S., Cole, C.G., Ward, S.A., Dunham, I., and Forbes, S.A. (2018). The COSMIC Cancer Gene Census: describing genetic dysfunction across all human cancers. Nat. Rev. Cancer 18, 696–705.

Sugiura, M., Kasama, Y., Araki, R., Hoki, Y., Sunayama, M., Uda, M., Nakamura, M., Ando, S., and Abe, M. (2014). Induced pluripotent stem cell generation-associated point mutations arise during the initial stages of the conversion of these cells. Stem Cell Rep. 2, 52–63.

Takahashi, K., and Yamanaka, S. (2006). Induction of pluripotent stem cells from mouse embryonic and adult fibroblast cultures by defined factors. Cell 126, 663–676.

Tarasov, A., Vilella, A.J., Cuppen, E., Nijman, I.J., and Prins, P. (2015). Sambamba: fast processing of NGS alignment formats. Bioinformatics 31, 2032–2034.

Thompson, O., von Meyenn, F., Hewitt, Z., Alexander, J., Wood, A., Weightman, R., Gregory, S., Krueger, F., Andrews, S., Barbaric, I., et al. (2020). Low rates of mutation in clinical grade human pluripotent stem cells under different culture conditions. Nat. Commun. 11, 1–14.

Thorvaldsdóttir, H., Robinson, J.T., and Mesirov, J.P. (2013). Integrative genomics viewer (IGV):

high-performance genomics data visualization and exploration. Brief. Bioinform. *14*, 178–192.

Warlich, E., Kuehle, J., Cantz, T., Brugman, M.H., Maetzig, T., Galla, M., Filipczyk, A.A., Halle, S., Klump, H., Schöler, H.R., et al. (2011). Lentiviral vector design and imaging approaches to visualize the early stages of cellular reprogramming. Mol. Ther. *19*, 782–789.

Wickham, H. (2016). ggplot2 (Springer International Publishing).

Williams, N., Lee, J., Moore, L., Baxter, E.J., Hewinson, J., Dawson, K.J., Menzies, A., Godfrey, A.L., Green, A.R., Campbell, P.J., et al. (2020). Phylogenetic reconstruction of myeloproliferative neoplasm reveals very early origins and lifelong evolution. bioRxiv, 2020.11.09.374710.

Yamanaka, S. (2020). Pluripotent stem cell-based cell therapy-promise and challenges. Cell Stem Cell *27*, 523–531.

Yates, A., Beal, K., Keenan, S., McLaren, W., Pignatelli, M., Ritchie, G.R.S., Ruffier, M., Taylor, K., Vullo, A., and Flicek, P. (2015). The Ensembl REST API: Ensembl Data for Any Language. Bioinformatics *31*, 143–145.

STAR★METHODS

KEY RESOURCES TABLE

REAGENT or RESOURCE	SOURCE	IDENTIFIER
Antibodies		
CD34-BV421, clone 561	Biolegend	Cat# 343609; RRID: AB_2561358
CD38-PE, clone HIT2	Biolegend	Cat# 303505; RRID: AB_314357
CD45RA-PerCp/Cy5.5, clone HI100	Biolegend	Cat# 304121; RRID: AB_893358
CD49f-PE/Cy7, clone GoH3	Biolegend	Cat# 313622; RRID: AB_2561705
CD90-APC, clone 5E10	Biolegend	Cat# 328113; RRID: AB_893440
Lineage(CD3/CD14/CD19/CD20/CD56)-FITC, clones UCHT1, HCD14,HIB19, HCD56)	Biolegend	Cat# 348701; RRID: AB_10644012
CD11c-FITC, clone 3.9	Biolegend	Cat# 301603; RRID: AB_314173
CD16-FITC, clone 3G8	Biolegend	Cat# 302005; RRID: AB_314205
Anti-Rabbit igG AF594	Invitrogen	Cat#855; RRID:2165334
Rabbit anti-pH3	Merck Milipore	Cat# 06-570; RRID: AB_310177
Biological samples		
Fetal tissue	Leiden University Medical center	Not applicable
Chemicals, peptides, and recombinant proteins		
Recombinant human thrombopoietin (TPO)	Preprotech	Cat# 300-18
Recombinant human stem cell factor (SCF)	Preprotech	Cat# 300-07
Recombinant human FLT3-L	Preprotech	Cat# 300-19
Recombinant human IL-6	Preprotech	Cat# 200-06
Recombinant human IL-3	Preprotech	Cat# 160-01
BSA	Sigma- Aldrich	Cat# A7030-10G
HEPES	Thermo-Fisher Scientific	Cat# 15630106
Penicillin-streptomycin (10.000U/ml)	Thermo-Fisher Scientific	Cat#15140122
GlutaMAX supplement	Thermo-Fisher Scientific	Cat#35050061
PBS	Thermo-Fisher Scientific	Cat# 14190
EDTA	Sigma- Aldrich	Cat# T4049
Primocin	Invivogen	Cat# ant-pm-1
SB 202190 monohydrocholoride hydrate	Sigma- Aldrich	Cat#S7076-5MG
B27 supplement	Thermo-Fisher Scientific	Cat#175044
N-Acetyl-cysteine	Sigma- Aldrich	Cat#A9165
A83-01	Tocoris	Cat#239/10
Y-27632 dihydrochloride	Abmole	Cat#M1817
Human EGF	Preprotech	Cat#AF-100-15
Nicotinamide	Sigma- Aldrich	Cat#N0636
WNT surrogate-fc fusion protein	U-protein express	Cat#N001
FBS	Sigma- Aldrich	Cat# A4766801
Clostridium histolyticum type IA	Sigma- Aldrich	Cat# C9891
DNase I	Sigma- Aldrich	Cat# DN25
EBSS	Thermo-Fisher Scientific	Cat#24010043
Revitacell supplement	Thermo-Fisher Scientific	Cat#A2644501
Triton X-100	Thermo-Fisher Scientific	Cat#85111

Continued

REAGENT or RESOURCE	SOURCE	IDENTIFIER
Fluormount-G Mounting Medium	Thermo-Fisher Scientific	Cat#00-4958-02
Advanced DMEM/F-12	Thermo-Fisher Scientific	Cat#12634028
Critical commercial assays		
QIAamp DNA Micro kit	QIAgen	Cat# 56304
Genomic tip 20/G	QIAgen	Cat#10223
Dneasy blood & tissue kit	QIAgen	Cat#69504
Rneasy mini kit	QIAgen	Cat#74004
Essential 8 flex medium kit	Thermo-Fisher Scientific	Cat#A2858501
Click-iT EdU Alexa Fluor 488 cell proliferation kit for imaging	Thermo-Fisher Scientific	Cat#10337
Deposited data		
Whole-genome sequence data from this article	This paper	European Genome-Phenome Archive(EGA; https://ega-archive.org/ega/home). Accession Number EGA: EGAS00001005939
Deep targeted re-sequencing	This paper	European Genome-Phenome Archive(EGA; https://ega-archive.org/ega/home). Accession Number EGA: EGAS00001005939
Whole-genome sequencing data	(Hasaart et al., 2020)	European Genome-Phenome Archive(EGA;https://ega-archive.org/ega/home). Accession Number EGA: EGAS00001003982 and EGAS00001002886
RNA sequencing data from this article	This paper	European Genome-Phenome Archive(EGA;https://ega-archive.org/ega/home). Accession Number EGA: EGAS00001005939
RNA sequencing data	(Kuijk et al., 2020)	European Genome-Phenome Archive(EGA; https://ega-archive.org/ega/home). Accession Number EGA: EGAS00001002955, EGAS00001000881 and EGAS00001001682
Software and algorithms		
Whole genome sequencing read alignment and mutation calling pipeline	Not applicable	https://github.com/UMCUGenetics/IAP https://github.com/UMCUGenetics/NF-IAP
RNA sequencing read alignment and mutation calling pipeline	Not applicable	https://github.com/UMCUGenetics/RNASeq-NF
SNV filtering pipeline	Not applicable	https://github.com/ToolsVanBox/SMuRF/
Indel filtering pipeline	Not applicable	https://github.com/ToolsVanBox/SMuRF/
R (v3.6)		https://www.r-project.org/
ggeffects R package (v0.14.2)	(Lüdecke, 2018)	https://cran.r-project.org/web/packages/ggeffects/index.html
ggplot2 R package (v3.2.1)	(Wickham, 2016)	https://cran.r-project.org/web/packages/ggplot2/index.html
Burrows-Wheeler Aligner mapping tool (v0.7.5a and v0.7.17)	(Li and Durbin, 2010)	https://github.com/lh3/bwa
DESeq2	(Love et al., 2014)	https://bioconductor.org/packages/release/bioc/html/DESeq2.html
GATK HaplotypeCaller (v3.8-1-0 and v4.1.3.0)	(DePristo et al., 2011)	https://gatk.broadinstitute.org/hc/en-us
Single Nucleotide Polymorphism Database (v146)	(Smigielski et al., 2000)	https://www.ncbi.nlm.nih.gov/snp/
Bedtools	(Smigielski et al., 2000)	https://bedtools.readthedocs.io/en/latest/
NimbleDesign Software	Not applicable	https://sequencing.roche.com/en/support-resources/discontinued-products/nimble-design-software.html

Continued

REAGENT or RESOURCE	SOURCE	IDENTIFIER
Integrative Genomics Viewer (IGV)	(Thorvaldsdóttir et al., 2013)	https://software.broadinstitute.org/software/igv/download
SAMTOOLS	(Li et al., 2009)	http://www.htslib.org/
deepSNV (v1.32.0)	(Gerstung et al., 2014)	https://bioconductor.org/packages/release/bioc/html/deepSNV.html
Cosmic cancer gene Census (v88)	(Sondka et al., 2018)	https://cancer.sanger.ac.uk/census
Ape (v5.5)	(Paradis et al., 2004)	http://ape-package.ird.fr/
Ensembl REST API	(Yates et al., 2015)	https://rest.ensembl.org/documentation/info/assembly_map
snpEFF (v4.1)	(Cingolani et al., 2012)	http://pcingola.github.io/SnpEff/
Sambamba (v0.6.8)	(Tarasov et al., 2015)	https://github.com/biod/sambamba/releases
Freec (v11.5)	(Boeva et al., 2012)	https://github.com/BoevaLab/FREEC
FastQC (v0.11.5)	Not applicable	https://www.bioinformatics.babraham.ac.uk/projects/fastqc/
MultiQC (v1.5)	(Ewels et al., 2016)	https://multiqc.info/
MutationalPatterns R package (v3.13)	(Blokzijl et al., 2018)	https://bioconductor.org/packages/release/bioc/html/MutationalPatterns.html

RESOURCE AVAILABILITY

Lead contact

Further information and requests for resources and reagents should be directed to and will be fulfilled by the lead contact, Ruben van Boxtel (R.vanboxtel@prinsesmaximacentrum.nl).

Materials availability

This study did not generate new unique reagents.

Data and code availability

Data: WGS, RNAseq and targeted re-sequencing data have been deposited at EGA (https://www.ebi.ac.uk/ega/), and accession numbers are listed in the key resources table. They are available upon request if access is granted. To request access, contact EGA.

In addition, tools used to process this data have been deposited at https://github.com/ToolsVanBox/ and are publicly available as the date of publication. The accension numbers are also listed in the key resources table. Microscopy data will be shared upon request. To request access, Ruben van Boxtel, R.vanboxtel@prinsesmaximacentrum.nl.

Code: Most code has been deposited at https://github.com/ToolsVanBox/ and in the MutationalPatterns R package and is publicly available as of the date of publication. DOIs are listed in the key resources table. Additional scripts will be shared upon request.

Any additional information required to reanalyze the data reported in this paper is available from the lead contact upon request.

EXPERIMENTAL MODEL AND SUBJECT DETAILS

For this study, we collected two T21 fetuses (gestational age (GA) 12 and 14.5) and two karyotypically normal fetuses (GA 14 and 16). The same fetuses were used for our previous study (Hasaart et al., 2020). The GA in weeks was determined by the measurement of first-trimester crown-rump length by ultrasonography. The age in weeks after conception was determined by subtracting 2 weeks of the GA. Fetal material was collected and disassociated as described before (Hasaart et al., 2020). Collection of material for this study (P08.087) was approved by the Medical Ethical Committee of the Leiden University Medical Center. The study was performed in accordance with the guidelines and regulations of the Helsinki declaration and

its later amendments or comparable ethical standards. Details of all samples are depicted in Table S1. Fetal ISC and iPSC cultures were generated from the fetuses described above.

METHOD DETAILS

Isolation and clonal cultures of HSPCs

Mononuclear cells were flushed out from fetal bone marrow. Single liver cells and mononuclear fetal bone marrow cells were stained with an antibody cocktail as described before (Hasaart et al., 2020; Huber et al., 2019). CD34+ and lineage- cells were single cell sorted in a 384 wells plate and cultured for 3-4 weeks in StemSpan SFEM medium supplemented with growth factors as described before (Hasaart et al., 2020). Cells were spun down and DNA was isolated as described in the section 'Genomic DNA isolation' in order to perform WGS.

Intestinal organoid cultures

Fetal intestine was disassociated into a single cell solution using collagenase type 1A (Sigma-Aldirch) and 0.1mg/ml DNaseI (Sigma-Aldrich) as described before (Hasaart et al., 2020). Single intestinal cells were plated in Matrigel droplets (Corning) and plated in limited dilution. Clonal ISC cultures were generated as described before and cultured in human ISC organoid (CHIO) medium (Hasaart et al., 2020). After a culture period of 1.5 month, sub-clonal ISC cultures were generated as described before (Jager et al., 2017). In short, ISC organoid were made single cell with tryplE, single ISC were sorted with the Sony SH800S in a tube based on FSC and SSC and plated in limited dilution in Matrigel (Corning) droplets.

iPSC culture

Bulk ISC cultures were made single cell using tryplE (thermo fisher). 20.000 Single ISCs were resuspended in 1 ml CHIO medium supplemented with 10 μM Rho kinase inhibitor (Abmole) and 4 mg/ml polybrene. 10.000 cells were plated in Matrigel coated plates diluted in Advanced DMEM/F-12 supplemented with 1% penicillin/streptomycin, 1% GlutaMAX, and 1% HEPES 10 mM. Cells were transduced with a third generation lentiviral vector containing Oct4, Klf4, Sox2, c-Myc, dTomato (Warlich et al., 2011). Cells were cultured in CHIO medium supplemented with 10 μM Rho kinase inhibitor and polybrene. After 3 days, medium was replaced with Essential E8 Flex medium (Thermo Scientific). RNA seq analysis confirmed that reprogramming was successful.

To make clonal iPSC lines, cells were made single cell with tryplE. After, single iPSCs were plated in limited dilution in a 96-well tissue culture plate coated with 100ul Matrigel diluted in in Advanced DMEM/F-12 supplemented with 1% penicillin/streptomycin, 1% GlutaMAX, and 1% HEPES 10 mM (1:40). To enhance cell survival after the clonal steps, Essential E8 flex medium was supplemented with RevitaCell (Thermo Scientific). Clonal iPSC lines were cultured and passaged under reduced oxygen conditions (3% O_2) to allow mutations to accumulate. To prevent changes in oxygen levels, cells were placed in CondoCells. Cells were passaged 2 times a week with 0.5mM EDTA. After a culture period of approximately 3 months, a second clonal step was performed.

Cell cycle length of iPSCs

The length iPSC cultures was determined by pulse-chase of 5-ethynyl-2′-deoxyuridine (EdU) and co-staining for the mitosis phosphorylated histone 3 (pH3). iPSCs were labeled with 10 mM EdU (Alexa Fluor 488 Imaging kit, Life Technologies EdU kit) for 30 minutes. After, cells were washed two times with PBSO and medium was replaced with fresh Essential E8 Flex medium. Chase was performed 2, 6, 9.5, 15, 19, 23, 28, 33.5, 39, 43 and 47 hours after washing. Cells were made single cell with tryplE. For each time point two times 50.000 single cells were cytospun (1000 rpm, 5minutes). Cells were fixed with 4%PFA, permeabilized with 0.1% Triton X100/TBS and blocked with 1% BSA TBST. Cells were stained with rabbit anti-pH3 (Merck Millipore, 1:500) overnight at 4 degree and with Alexa 594-conjugated donkey anti rabbit (Invitrogen, 1:500). Afterward, EdU detection was performed with Click-iT assay following the manufacturer's manual. iPSCs were mounted with DAPI and Fluoromount, and imaged with the Leica Thunder microscope. Per condition the full slide was imaged and analyzed with Fiji software and Rstudio.

RNA sequencing

iPSC cell pellets and ISC cell pellets were snap frozen and RNA was isolated using the RNeasy mini kit (Qiagen). RNA extractions were performed according to manufacturers' instructions. RNA quality was

measured with the bioanalyzer. polyA tail libraries were generated from 200ng input RNA. Libraries were sequenced using the NextSeq2000 (2x 50 bp). RNA sequencing reads were aligned to human reference genome GRCh38 using the STAR algorithm. Full pipeline description and settings are available at https://github.com/UMCUGenetics/RNASeq-NF. Read counts were normalized using DESeq2 package version 1.32.0 (Love et al., 2014). Downstream analysis, including differential expression analysis and hierarchical clustering, were performed with DESseq2 package version 1.32.0 as well. The dds object was transformed using the function vst and heatmaps were produced by normalizing the expression mean to 0. Count tables of H9 ES cells were obtained from a previously published study and used to compare the transcriptional profile of the generated iPSCs with the transcriptional profile of H9 ES cells (Kuijk et al., 2020).

Genomic DNA isolation

Genomic tip 20/G (Qiagen) was used to extract DNA from bulk skin tissue, ISC organoid cultures and spleen. DNA from clonal HSPCs cultures was extracted using Qiamp DNA Micro Kit (Qiagen). The blood and tissue kit (Qiagen) was used to extract DNA from clonal iPSC and cultures. All DNA isolations were performed according to manufacturers' instructions.

Whole genome sequencing and read alignment

In addition to the data described below, WGS data from a previously published study was used (Hasaart et al., 2020). DNA libraries for Illumina sequencing were generated using standard protocols (Illumina). Libraries were generated from 300-500 ng of genomic DNA isolated from clonal iPSC cultures and ISC organoid cultures. For the clonal HSPC culture, 50-100 ng genomic DNA was used as input. All samples were sequenced (2 × 150 bp) using NovaSeq 6000 sequencers to 15X base coverage except for the sub-clonal ISC cultures and DNA of bulk skin these were sequenced 30X base coverage. DNA of bulk skin was sequenced twice 30X base coverage. WGS data was mapped against human reference genome GRCh38 using Burrows-Wheeler Aligner v0.7.5a mapping tool (Li and Durbin, 2010) with settings 'bwa mem -c 100 -M'. Sequence reads were marked for duplicates using Sambamba v0.6.8 markdup. Full pipeline description and settings are available at: https://github.com/UMCUGenetics/IAP.

For the clonal iPSC and sub-clonal ISC cultures, Burrows-Wheeler Aligner v0.7.17 was used (https://github.com/ToolsVanBox/NF-IAP/).

Somatic mutation calling and filtering

Raw variants were multisample-called using the GATK HaplotypeCaller v3.8-1-0 (DePristo et al., 2011) and GATK Queue v3.8-1-0 with default settings and the additional option 'EMIT_ALL_CONFIDENT_SITES'. The quality of variants and reference positions was evaluated by GATK VariantFiltration v3.8-1-0 with options -snpFilterName SNP_LowQualityDepth -snpFilterExpression "QD < 2.0" -snpFilterName SNP_MappingQuality -snpFilterExpression "MQ < 40.0" -snpFilterName SNP_StrandBias - snpFilterExpression "FS > 60.0" -snpFilterName SNP_HaplotypeScoreHigh -snpFilterExpression "HaplotypeScore > 13.0" -snpFilterName SNP_MQRankSumLow -snpFilterExpression "MQRankSum < -12.5" -snpFilterName SNP_ReadPosRankSumLow -snpFilterExpression "ReadPosRankSum < -8.0" -snpFilterName SNP_HardToValidate -snpFilterExpression "MQ0 >= 4 && ((MQ0 / (1.0 * DP)) > 0.1)" -snpFilterName SNP_LowCoverage -snpFilterExpression "DP < 5" - snpFilterName SNP_VeryLowQual -snpFilterExpression "QUAL < 30" -snpFilterName SNP_LowQual -snpFilterExpression "QUAL >= 30.0 && QUAL < 50.0 " -snpFilterName SNP_SOR -snpFilterExpression "SOR > 4.0" -cluster 3 -window 10 -indelType INDEL -indelType MIXED - indelFilterName INDEL_LowQualityDepth -indelFilterExpression "QD < 2.0" -indelFilterName INDEL_StrandBias -indelFilterExpression "FS > 200.0" -indelFilterName. INDEL_ReadPosRankSumLow -indelFilterExpression "ReadPosRankSum < -20.0" -indelFilterName INDEL_HardToValidate -indelFilterExpression "MQ0 >= 4 && ((MQ0 / (1.0 * DP)) > 0.1)" - indelFilterName INDEL_LowCoverage -indelFilterExpression "DP < 5" -indelFilterName INDEL_VeryLowQual -indelFilterExpression "QUAL < 30.0" -indelFilterName INDEL_LowQual - indelFilterExpression "QUAL >= 30.0 && QUAL < 50.0" -indelFilterName INDEL_SOR - indelFilterExpression "SOR > 10.0". For the clonal iPSC and sub-clonal fetal ISC cultures, GATK v4.1.3.0 was used with the same settings. To obtain high-quality somatic mutation catalogs, we applied postprocessing filters as described (Blokzijl et al., 2016). Briefly, we considered variants at autosomal chromosomes without any evidence from a paired control sample (skin); passed by VariantFiltration with a GATK phred-scaled quality score R 100; a base coverage of at least 5X in the clonal and paired control sample; mapping quality (MQ) of 60; no overlap with single nucleotide polymorphisms (SNPs) in the Single Nucleotide Polymorphism Database v146; and absence of the variant

in a panel of unmatched normal human genomes (BED-file available upon request). We additionally filtered base substitutions with a GATK genotype score (GQ) lower than 99 or 10 in clonal or paired control sample, respectively. For indels, we filtered variants with a GQ score lower than 99 in both clonal and paired control sample (Blokzijl et al., 2016; Jager et al., 2017). We used Bayesian Dirichlet modeling to check the clonality of the clones, as described before (Hasaart et al., 2020; Nik-Zainal et al., 2012). Mutations with a VAF > 0.3 were assumed to be clonal. Mutations located in protein coding regions were annotated with snpeff (v4.1).

A mutation was considered as potential cancer driver if it met two requirements. First it needed to be annotated with "MODERATE" or "HIGH" effect based on the effect impact criteria of snpEff v4.1 (Cingolani et al., 2012) and second it needed to be annotated in the Cosmic cancer gene census (v88).

To assess somatic mutations from our previous published study, we converted the VCFs to human reference genome GRCh38 (Hasaart et al., 2020), using Ensembl REST API (https://rest.ensembl.org/documentation/info/assembly_map).

To determine the mutations acquired during iPSC or ISC culture we subtracted all clonal mutations in the parental clone from the clonal mutations in the sub-clone.

Mutations were manually inspected using IGV to exclude false positives calls and include false negative calls.

Targeted deep re-sequencing

Genomic DNA of bulk skin, bulk ISC organoid cultures passage 0 and spleen were subjected to targeted deep re-sequencing. A bait set, containing all somatic mutations identified with WGS was designed using NimbleDesign Software. DNA libraries were generated from 200ng genomic DNA using TruSeq Nano DNA library prep kit according to manufacturers' instructions. DNA libraries were pooled and DNA regions of interest were captured from a 1000 ng pooled library using SeqCap EZ Hypercap (Roche). DNA libraries were sequenced (2 x 150 bp) using Nextseq500.

WGS data was aligned against the human reference genome GRCh37 with the same methods as described previously. Further bioinformatic analyses were performed using the R language. Reads were loaded using the loadAllData function from the deepSNV (v 1.32.0) R package, using q=30 and mq=30 (Gerstung et al., 2014). After, the betabinLRT function from the same package was used with rho=1e-4, maxtruncate=1 and truncate=1 to run a maximum likelihood version of the Shearwater algorithm. Next, Benjamini and Hochberg multiple testing correction was performed on the resulting p-values (Benjamini and Hochberg, 1995). The qvals2Vcf function with standard settings was used to generate a vcf file. Next, variants were filtered in several steps. First, variants were the reference and alternative alleles were the same were removed. After this, variants were the reference allele was set to "-" were filtered out. Variants within 10bp of an indel were removed. Next, only variants that were present in both the bulk skin and bulk ISC of a single sample were retained. Finally, for each fetus we only took the variants that matched the variants found in the WGS data of the clones.

After we converted the obtained VCFs to human reference genome GRCh38 , using Ensembl REST API (https://rest.ensembl.org/documentation/info/assembly_map).

Construction of developmental lineage tree

Developmental lineage trees were constructed as described before (Hasaart et al., 2020). Somatic mutations sub clonally present in bulk skin were included and represent early embryonic mutations. The relationship between clones deducted from the shared and unique somatic mutations were visualized with the ape package.

Mutation rate during early embryogenesis

The number of SNVs per branch of the developmental lineage tree were counted. To ensure we assessed mutations that occurred pre-gastrulation, only the early branches whose contribution summed to 100% were used. Because not all cells were assessed, either because they were not sampled or because they were lost during development, a single branch can contain multiple cell divisions. The VAF was used to determine if the mutations in a branch occurred during a single cell division. In ambiguous cases, a Chi-square test with a simulated p-value (k=2000), was performed on the reference- and alternative allele counts of all mutations in a branch. If the VAFs between mutations were significantly different, then the

mutations occurred during multiple cell divisions. Based on the number of mutations per branch, the average number of mutations per cell division was calculated. This analysis was done separately for both the targeted mutations and the mutations that were identified in the fetal clones.

Mutation rate of iPSCs and ISCs

Culture-associated SNVs and indels were identified by subtracting the clonal mutations present in de sub clone from the clonal mutations present in the matching-clone. Culture-associated SNVs and indels were pooled per clone. The culture-associated mutation rate of iPSCs and ISCs in each clone was calculated by the total number of culture-associated mutations, the number of days in culture and the average cell cycle length determined by pulse-chase of 5-ethynyl-2′-deoxyuridine (EdU) and co-staining for the mitosis phosphorylated histone 3 (pH3). The cell cycle length of ISCs in culture was obtained from a previously published study, which measured the cell cycle length with a similar approach (Drost et al.,2017).

Mutational profiles and signature analyses

We determined all somatic mutations, which are shared between tissues or cells from at least 2 different germ layers as somatic mutations acquired pre-gastrulation. For this we included: 1) shared somatic mutations between ISC and HSPC clones 2) somatic mutations present in bulk skin identified with WGS 3) somatic mutations shared between skin and bulk ISC passage 0 identified with targeted re-sequencing. Somatic mutations acquired pre-gastrulation of the 4 fetuses are pooled together, because of the low number of mutations. All somatic mutations were counted once. In addition, all culture-associated mutations in iPSCs were pooled together. Mutational profile and mutational signature analyses were performed on pooled samples with the new functions of the R package MutationalPatterns (release 3.13) https://github.com/ToolsVanBox/MutationalPatterns (Blokzijl et al., 2018). A chi squared test was performed on the 7-type mutation spectra to determine differences between the mutation spectra of cultured iPSCs and pluripotent embryonic cells *in vivo*. Mutational signature analyses was performed with the newest version of the COSMIC signatures (v 3.21) (Alexandrov et al., 2020). De novo mutational signature extraction was performed using the data reported here, in combination with genome-wide mutation data of healthy stem cells of human small intestine, colon and liver as described previously (Blokzijl et al., 2018; Osorio et al., 2018). We applied nonnegative matrix factorization and extracted 2 mutational signatures based on the residual sum of squares (RSS) plot and plot_original_vs_reconstructed function. The 2 de novo extracted signatures were compared to the COSMIC signatures and based on a cosine similarity being >0.85 were identified as SBS1 and SBS5. With these 2 signatures we performed a strict refit on the pooled samples with the fit_to_signatures_strict function with the setting max_delta=0.05 and best fit option.

QUANTIFICATION AND STATISTICAL ANALYSIS

Sample numbers used for statistical analysis are depicted in the figures.

To determine the somatic mutation rate pre-gastrulation, we used the VAF to determine if the mutations in a branch occurred during a single cell division. In ambiguous cases, a Chi-square test with a simulated p-value (k=2000), was performed on the reference- and alternative allele counts of all mutations in a branch. If the VAFs between mutations were significantly different, then the mutations occurred during multiple cell divisions. A Wilcoxon rank-sum test was used to compare the mutation rate of iPSCs and embryonic cells pre-gastrulation, and to compare the culture-associated mutation rate of iPSCs and fetal ISCs.

A Chi-squared test was used to determine differences in the 7-mutation spectra of cultured iPSC and embryonic cell pre-gastrulation. We used the cosine similarity to compare the 96-mutational spectra of iPSCs and embryonic cells pre-gastrulation.